Convection in conditionally unstable seawater

Cite as: AIP Advances 11, 075324 (2021); doi: 10.1063/5.0053629
Submitted: 9 April 2021 • Accepted: 9 July 2021 •
Published Online: 23 July 2021

Jan Erik H. Weber[1,a)] and Göran Broström[2]

AFFILIATIONS

[1] Department of Geosciences, University of Oslo, Oslo, Norway
[2] Department of Marine Sciences, University of Gothenburg, Gothenburg, Sweden

[a)] Author to whom correspondence should be addressed: j.e.weber@geo.uio.no

ABSTRACT

Buoyancy-driven convection in a conditionally unstable ocean is studied theoretically. Conditionally unstable conditions are related to supercooled seawater. The freezing point is depressed due to increasing pressure, and upward motion (reduced pressure) leads to the formation of ice crystals in the form of frazil ice and hence a reduced bulk density of the rising mass parcel. For downward motion (increasing pressure), freezing does not occur. To model this one-way process, we take that rising parcels become lighter as they follow the adiabatic density lapse rate due to freezing. Through the action of a unit step function, we can model the fact that frazil ice is added only in the upward motion. Supercooled seawater is observed in the proximity of ice shelf fronts. We consider an idealized ice shelf and take the front to be vertical. For this geometry, we present linear analytical solutions as well as numerical results for nonlinear two-dimensional steady conditional convection in the presence of a stable environmental density gradient. With a parallel to moist convection in the atmosphere, we find convection cells near the ice front with rising fluid in a narrow region and sinking fluid over a much broader region.

I. INTRODUCTION

Rayleigh[1] convection between horizontal planes kept at different constant temperatures (a cold plane on the top) has attracted massive attention from researchers. For most problems studied, the instability is absolute in the sense that once a critical value of a certain dimensionless parameter (e.g., the Rayleigh number or the Marangoni number in the case with surface tension) is exceeded, the displacement of an individual particle in the gravity field is unstable regardless of whether the displacement is upward or downward. In cases when the basic density field is conditionally unstable, the situation is different. The particles that are displaced upward become lighter than the environment and will continue to ascend, while a particle that is displaced downward will tend to be restored and move back to the equilibrium position. Hence, upward motion is unstable, and downward motion is stable. Such situations may be found when we have phase transitions in the fluid.

In the atmosphere, this is known as moist convection. Due to the compressibility of the air, convective instability occurs only if the numerical value of the environmental temperature gradient is larger than the adiabatic lapse rate. However, lifting moist air parcels will imply some degree of condensation of water vapor within the parcel and hence a temperature increase due to the release of latent heat. That means that the adiabatic temperature decrease with height is somewhat smaller for a moist parcel than for a dry one. For downward motion, there is no condensation within the moist parcel, and moist and dry parcels tend to follow the dry adiabatic lapse rate. Hence, if the environmental temperature gradient lies between the moist adiabatic lapse rate (typically 0.6 K/100 m) and the dry adiabatic lapse rate (~1 K/100 m), the stratification is conditionally unstable.[2–6] For a comprehensive review of atmospheric moist convection, see Ref. 7.

In the Antarctic Ocean, Foldvik and Kvinge[8] discussed this phenomenon in connection with seawater being cooled by the presence of the Filchner ice shelf. Since the freezing temperature of seawater decreases with increasing pressure (i.e., depth), cold water parcels displaced upward toward lower pressure will tend to form small ice crystals. This, in turn, renders the bulk density of the parcel smaller and promotes further ascent. Parcels displaced downward will not form any ice and tend to move back to their original positions. The ice crystals considered by Foldvik and Kvinge[8] were observed in rising water, and not *in situ* within supercooled water.

However, Dieckmann *et al.*[9] have found ice platelets from hydrographic observations at 250 m depth near the Filchner ice shelf, showing that "underwater" ice is produced at these depths. More recently, observation of ice platelets in Antarctic waters was reported by Hunkeler *et al.*,[10] while several papers have modeled the growth of frazil ice in Antarctica.[11,12] Supercooled water, which is a necessary condition for frazil ice formation, has also been observed near a glacier in Spitsbergen[13,14] as well as in an Arctic polynia.[15]

Foldvik and Kvinge[8] studied this process by considering the adiabatic motion of an individual fluid parcel in the absence of viscosity and diffusion. A more comprehensive study of conditional frazil ice instability in seawater is found in the study by Jordan *et al.*,[16] where the stability analysis is formulated as a general perturbation problem. In this paper, the frazil ice formation related to rising fluid parcels is calculated by assuming adiabatic processes.[8] In the perturbation equation for density, we introduce a Heaviside step function to account for the differences in buoyancy-forcing when the vertical velocity w is upward ($w > 0$) and when it is downward ($w < 0$). A similar approach has been used in atmospheric applications to account for the release of latent heat in ascending moist air.[17–19]

The application of a step function to model conditional instability is novel for the ocean. It makes it possible to mathematically investigate not only the growth rates of unstable modes but also the onset of linear convective motion through marginal stability (zero growth rate), as well as the steady finite amplitude cellular motion in a conditionally unstable fluid layer. These are new results that shed light on an important dynamical process in supercooled seawater.

The rest of this paper is organized as follows: In Secs. II–IV, we develop the governing equations for this problem. Particular emphasis is put on the density equation and the form of the Heaviside function that is chosen to model the effect of conditional instability. Section V describes the ice shelf model and the boundary conditions. In Sec. VI, we discuss the linear problem, which is solved by matching solutions in the unstable and stable regions. Section VII presents numerical solutions for nonlinear conditional instability in a thin layer, and Sec. VIII contains a discussion and some concluding remarks.

II. GOVERNING EQUATIONS

We consider density-driven motion in a horizontal layer of ocean water with depth H. The horizontal x, y axes are placed at the lower boundary, and the vertical z axis is positive upward. The ocean is stratified due to gradients of heat, salt, and ice crystals. In general, the equation of state can be written as

$$\rho = \rho(p, T, S, C), \tag{1}$$

where ρ is the density, p is the pressure, T is the temperature, and S is the salinity. Furthermore, C is the dimensionless concentration of ice crystals (volume of ice per unit volume of the ice–seawater mixture). The velocity vector is $\boldsymbol{v} = (u, v, w)$, and the conservation of mass is governed by

$$\rho \nabla \cdot \boldsymbol{v} = -D\rho/Dt. \tag{2}$$

Here, ∇ is the gradient operator, t denotes time, and $D/Dt = \partial/\partial t + \boldsymbol{v} \cdot \nabla$ is the material derivative.

Following the study by Spiegel and Veronis,[20] any of the variables F in (1) is written as

$$F = F_m + F_0(z) + F'(x, y, z, t). \tag{3}$$

Here, the subscript m denotes constant mean reference values, and subscript 0 is related to the deviations from the mean values in the equilibrium state prior to motion. The primed quantities are space and time dependent fluctuations related to the convective motion. The analysis that follows is based on the assumption that

$$|F'| \le \Delta F_0 \ll F_m, \tag{4}$$

where ΔF_0 is the maximum difference in the equilibrium state across the layer. The scale heights D_F of this problem can be defined as

$$D_F = F_m |dF_0/dz|^{-1}. \tag{5}$$

Utilizing (4) and assuming that the layer thickness H is much less than the smallest scale height (5) and that the velocity in the fluid is much smaller than the speed of sound, the Boussinesq approximation is verified for a compressible fluid.[20] By defining the dimensionless perturbation density σ' as

$$\sigma' = \rho'/\rho_m, \tag{6}$$

the conservation of momentum and mass for a Boussinesq fluid reduces to

$$D\boldsymbol{v}/Dt = -\nabla p'/\rho_m - g\sigma' \boldsymbol{k} + \nu \nabla^2 \boldsymbol{v}, \tag{7}$$

$$\nabla \cdot \boldsymbol{v} = 0, \tag{8}$$

where g is the acceleration due to gravity, ν is the (constant) eddy viscosity, $\boldsymbol{k}$ is the vertical unit vector, and ∇^2 is the Laplacian operator. Here, we have neglected the effect of the rotation of the Earth since the fluid domain near the ice shelf front is relatively small.

For our purpose, the equation of state (1) for the two-component mixture of seawater and ice crystals will be written as[21]

$$\rho = \rho_m(1 - C)[1 - \alpha_m(T - T_m) + \beta_m(S - S_m)] + \rho_i C, \tag{9}$$

where ρ_i is the density of ice. Here, the expansion coefficients α_m and β_m are defined as

$$\alpha_m = -\left(\rho^{-1}\partial\rho/\partial T\right)_m, \quad \beta_m = \left(\rho^{-1}\partial\rho/\partial S\right)_m. \tag{10}$$

From the study by Spiegel and Veronis,[20] an equation for the perturbation temperature is obtained from the internal energy equation in the fluid (see also the study by Løyning and Weber).[22] Applying (3)–(5), one finds for the water phase that

$$DT'/Dt + [dT_0/dz + \Gamma]w = \kappa_T \nabla^2 T' + q'_T. \tag{11}$$

Here, q'_T is a source term for energy. Furthermore, $\Gamma = \alpha_m T_m g/c_p$ is the adiabatic temperature lapse rate for seawater,[22] where c_p is the specific heat capacity at constant pressure. In the upper ocean, the adiabatic lapse rate due to thermal expansion is very small, and this effect will be neglected in the forthcoming analysis. Accordingly, we disregard Γ in (11). Similarly, the salinity equation for seawater can be written as

$$DS'/Dt + [dS_0/dz]w = \kappa_S \nabla^2 S' + q'_S, \tag{12}$$

where q_S' is a source term for salt. Assuming vanishing mean ice concentration in the basic state, for the ice concentration perturbation, we can write

$$DC'/Dt = \kappa_C \nabla^2 C' + q_C', \tag{13}$$

where q_C' is a source term related to the formation of frazil ice. We take that the turbulent diffusion coefficients for heat, salt, and ice concentration in (11)–(13) are equal in this problem, i.e., $\kappa_T = \kappa_S = \kappa_C = \kappa$. Then, we avoid any double-diffusive convective processes, which are not a theme here.

In the equation of state (9), we take that $C_0(z) = 0$ and $|C'| \ll 1$. Hence, for the basic environmental stratification in the fluid, we can write

$$d\rho_0/dz = -\rho_m \alpha_m dT_0/dz + \rho_m \beta_m dS_0/dz, \tag{14}$$

while neglecting small products of primed quantities, the perturbation density becomes

$$\rho' = \rho_m(-\alpha_m T' + \beta_m S') - (\rho_m - \rho_i)C'. \tag{15}$$

In the last term, we have assumed that $\rho_0 \approx \rho_m$. Multiplying (11) by $-\rho_m \alpha_m$, (12) by $\rho_m \beta_m$ and (13) by $-(\rho_m - \rho_i)$, we find by adding these equations and utilizing (14) and (15),

$$D\sigma'/Dt + \left[\frac{1}{\rho_m} d\rho_0/dz\right] w = \kappa \nabla^2 \sigma' - Q', \tag{16}$$

where

$$Q' = \alpha_m q_T' - \beta_m q_S' + (\rho_m - \rho_i) q_C'/\rho_m. \tag{17}$$

III. THE INSTABILITY MECHANISM

The fundamental process in this problem is the generation of perturbation density σ' in (16) due to frazil ice formation in supercooled seawater. We take that the basic environmental density gradient in (16) can be written as

$$d\rho_0/dz = \Delta\rho/H, \tag{18}$$

where $\Delta\rho$ is a constant. The equation governing the density perturbation then becomes

$$D\sigma'/Dt + [\Delta\rho/(\rho_m H)]w = \kappa \nabla^2 \sigma' - Q'. \tag{19}$$

Here, Q', defined by (17), is the source of perturbation buoyancy caused by the phase transition. In this process, the liberation of latent heat and excess salinity is less effective than the ice crystal formation.

We assume that all upward motion causes freezing and that individual fluid parcels, containing a mixture of seawater and ice crystals, move as a bulk volume. Utilizing the hydrostatic equation and assuming that the seawater is sufficiently supercooled, we find from the calculations in the study by Foldvik and Kvinge[8] [Eq. (10)] that the frazil ice concentration in a fluid parcel moved adiabatically upward increases with height according to

$$(dC'/dz)_{ad} = 9.3 \times 10^{-6} \mathrm{m}^{-1}. \tag{20}$$

The corresponding density decrease due to freezing becomes

$$(d\sigma'/dz)_{ad} = -\gamma, \tag{21}$$

where

$$\gamma = 9.3 \times 10^{-7} \mathrm{m}^{-1}, \tag{22}$$

is the adiabatic density lapse rate. Hence, supercooled parcels moved adiabatically upward experience a decrease in density according to (21). For parcels moving downward, there is no freezing, and $(d\sigma'/dz)_{ad} = 0$ (it should be noted that the displacements cannot be exactly adiabatic due to the inclusion of dissipative terms). To model this one-way process, we may write Q' as

$$Q' = w\gamma U(w), \tag{23}$$

where $U(w)$ is the unit step function (Heaviside's unit function) defined by

$$U(w) = \begin{cases} 1, w > 0, \\ 0, w < 0. \end{cases} \tag{24}$$

In this way, ice crystals are only added in upward motion. A similar approach has been used for moist convection in the atmosphere.[17–19] By inserting (23) into (19), we find

$$D\sigma'/Dt + [\Delta\rho/(\rho_m H) + \gamma U(w)]w = \kappa \nabla^2 \sigma'. \tag{25}$$

In order to reveal the instability mechanism in this problem, we first simplify and disregard the diffusion term on the right-hand side of (25) (diffusion always acts stabilized by smearing out spatial density differences). Introducing the perturbation buoyancy force[23] per unit density

$$b = -g\sigma', \tag{26}$$

we find from (25) that

$$Db/Dt - Bw = 0, \tag{27}$$

where $B = g[\Delta\rho/(\rho_m H) + \gamma U(w)]$. Introducing a small vertical parcel displacement ζ such that $w = D\zeta/Dt$, (27) can be integrated, yielding

$$b = B\zeta. \tag{28}$$

Here, we have assumed that $b = 0$ when $\zeta = 0$. We thus notice from (28) that if $B > 0$, we have $b > 0$ when $\zeta > 0$ or $b < 0$ when $\zeta < 0$. Then, the buoyancy force acts in the same direction as the parcel displacement, which is a necessary condition for instability. On the other hand, when $B < 0$, buoyancy forces and displacements have opposite signs, characterizing a stable basic state.

In the absence of phase transitions ($\gamma = 0$), the environmental density gradient in (25) must be positive in order to promote convective instability ($B > 0$). When convection in this case occurs between horizontal parallel planes, we have the familiar Rayleigh–Benard problem;[1] see, for example, the review by Palm.[24] When phase transitions (frazil ice formation) occur in connection with ascending motion of fluid parcels, instability requires that in (25),

$$\gamma > -\Delta\rho/(\rho_m H). \tag{29}$$

From the study by Foldvik and Kvinge,[8] we assess the environmental density gradient per unit density in the upper 400 m to be

$$\left(H^{-1}\Delta\rho/\rho_m\right)_{env} \approx -4\times10^{-7}\,\mathrm{m}^{-1}. \tag{30}$$

Hence, the environmental density distribution acts stabilized, so the only possible mechanism for convective cell motion is conditional instability. From (22) and (30), we realize that the instability criterion (29) is fulfilled for this particular case. Hence, conditional instability can occur near the ice shelves in Antarctica. In the following sections, we analyze this problem quantitatively.

IV. NON-DIMENSIONAL GOVERNING EQUATIONS

We non-dimensionalize our problem by introducing

$$\begin{aligned}(x,y,z) &= (\hat{x},\hat{y},\hat{z})H,\\ t &= \hat{t}H^2/\kappa,\\ (u,v,w) &= (\hat{u},\hat{v},\hat{w})\kappa/H,\\ p' &= \hat{p}\rho_m\kappa\nu/H^2,\\ \sigma' &= \hat{\sigma}\kappa\nu/\left(gH^3\right),\end{aligned} \tag{31}$$

where variables with a caret are non-dimensional. Skipping carets, our governing equations in the non-dimensional form become

$$Pr^{-1}D\boldsymbol{v}/Dt = -\nabla p - \sigma\boldsymbol{k} + \nabla^2\boldsymbol{v}, \tag{32}$$

$$\nabla\cdot\boldsymbol{v} = 0, \tag{33}$$

$$D\sigma/Dt + \left[-R_N + R_\gamma U(w)\right]w = \nabla^2\sigma, \tag{34}$$

where $Pr = \nu/\kappa$ is the Prandtl number. In (34), we have defined

$$R_N = -gH^3\Delta\rho/(\rho_m\kappa\nu) = gH^4N^2/(\kappa\nu) > 0. \tag{35}$$

Here, N^2 is the squared buoyancy frequency for stable motion. The destabilizing parameter R_γ is defined by

$$R_\gamma = gH^4\gamma/(\kappa\nu). \tag{36}$$

In this problem, the effective Rayleigh number R for unstable motion becomes

$$R \equiv R_\gamma - R_N. \tag{37}$$

Due to the Heaviside function, (34) is nonlinear, even for infinitesimal disturbances. However, the linear stability problem can be analyzed by considering solutions in regions where $w > 0$ (unstable regions) and where $w < 0$ (stable regions) and then by matching the solutions where $w = 0$. Nonlinearly, the set of equations can be solved numerically without the need to consider separate regions, as shown in Sec. VII.

V. ICE SHELF MODEL

In this study, we consider convection in a very simple geometry. The ice shelf front is vertical and extends down to the horizontal continental shelf bottom; see Fig. 1. The horizontal extent is semi-infinite.

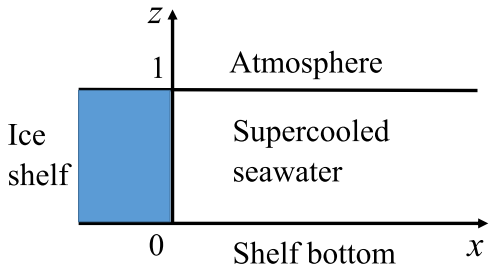

FIG. 1. Model geometry.

The horizontal boundaries are assumed to be impermeable planes, which for simplicity are taken to be perfectly "conducting." That means that any density perturbation will vanish at these boundaries. Mathematically, for the non-dimensional quantities,

$$w = \sigma = 0,\ z = 0,1. \tag{38}$$

To simplify the analytical analysis, we assume free-slip, i.e., $\partial u/\partial z = 0$, at the upper and lower boundary. Differentiating (33) with respect to z, in terms of the vertical velocity, we obtain[25]

$$\partial^2 w/\partial z^2 = 0,\ z = 0,1. \tag{39}$$

In the numerical analysis, we use the conventional no-slip conditions, which only yield small quantitative differences from free-slip.[25] We also neglect the effect of viscous drag at the vertical ice front, which means that

$$\partial w/\partial x = 0,\ x = 0. \tag{40}$$

In this problem, we realize that the water mass must be supercooled by the ice in order to produce ice crystals. Therefore, we are primarily interested in the region in the proximity of the vertical shelf. Here, we assume that the water is sufficiently mixed, yielding homogeneous conditions in the horizontal direction. Outside the region of ice crystal formation, there is no mean circulation in the vertical plane, and the variables tend to zero. Mathematically, this means that

$$u,\quad w,\quad \sigma \to 0,\quad x \to \infty. \tag{41}$$

However, in practice, our solutions tend to zero at a seaward distance, which is comparable to the shelf depth, as will be demonstrated in Sec. VI.

For a more realistic model of an Antarctic ice shelf, the supercooled water may come from a meltwater plume emerging from an ice-shelf cavity[21] rather than cooling from the side of an ice shelf front. A similar conclusion was reached by Morozov *et al.*[13] and Marchenko *et al.*[14] for supercooled seawater near the glacier front in a Spitsbergen fjord. However, the main focus of the present paper is on the fundamental dynamics of conditional convection, so we stick to the vertical front as the source of supercooling for computational simplicity.

VI. MATCHED LINEAR SOLUTIONS

We consider infinitesimal perturbations from the basic state, which allows us to linearize our equations, i.e., $\boldsymbol{v}\cdot\nabla\boldsymbol{v}$ and $\boldsymbol{v}\cdot\nabla\sigma$

are small and can be neglected in (32) and (34). For an analytical approach, it is convenient to divide our region into two parts: region 1 where $w > 0$ and region 2 in which $w < 0$. The analysis resembles that for the atmosphere.[3,5] We shall, therefore, only give a brief account of the coupling between marginally stable convection and a steady field of descending motion.

We perform the curl of (32) and use $w_z = -u_x$ for two-dimensional motion. Applying the Laplacian operator on this equation, we insert $\nabla^2\sigma$ from (34). For steady $(\partial/\partial t = 0)$ linear motion in the unstable region, (32)–(34) then reduce to

$$\nabla^6 w_1 - R\partial^2 w_1/\partial x^2 = 0, \ w_1 > 0, \tag{42}$$

where, as mentioned before, $R = R_\gamma - R_N$ is the effective Rayleigh number for this problem. In the stable region, we find that

$$\nabla^6 w_2 + R_N \partial^2 w_2/\partial x^2 = 0, \quad w_2 < 0. \tag{43}$$

The first four boundary conditions for the vertical velocity are stated in (38) and (39). They are

$$w_{1,2} = \partial^2 w_{1,2}/\partial z^2 = 0, \ z = 0, 1. \tag{44}$$

The last two boundary conditions are obtained from the linearized vorticity equation under the assumption of free-slip and perfectly conducting boundaries. Defining the vorticity $\eta = \partial w/\partial x - \partial u/\partial z$, from the linearized version of (32), we obtain

$$Pr^{-1}\partial\eta/\partial t = -\partial\sigma/\partial x + \partial^2\eta/\partial x^2 + \partial^2\eta/\partial z^2. \tag{45}$$

From our previous conditions, only the last term here is non-zero at the boundaries, yielding $\partial^3 u/\partial z^3 = 0$. By differentiating with respect to x and substituting from the continuity equation (33), we finally obtain the last two conditions,

$$\partial^4 w_{1,2}/\partial z^4 = 0, \ z = 0, 1. \tag{46}$$

In the unstable region, we have that the lowest marginally stable mode can be written in the normalized form,[25]

$$w_1 = \sin \pi z \cos kx. \tag{47}$$

The critical (minimum) Rayleigh number becomes

$$R = R_c = 27\pi^4/4 \tag{48}$$

for a critical wave number $k_c = \pi/2^{1/2}$. We have assumed that the vertical velocity is positive. That means that the half-cell of the ascending fluid must be confined to the region $0 \le x \le \pi/(2k)$. For the critical case, the non-dimensional width L of the half-cell then becomes $L = 2^{1/2}/2$.

The region of descending fluid in this problem is found to be $x \ge L = 2^{1/2}/2$. From (43), we realize that the x-part of the motion here cannot be represented by a Fourier component. For the first mode in the vertical region, we can write that $w_2 = \sin \pi z W(x)$, where

$$(D^2 - \pi^2)^3 W + R_N D^2 W = 0, \ x \ge L. \tag{49}$$

Here, $D = d/dx$. If we assume that $W \propto \exp[r(x - L)]$, the values of r are easily obtained from (49). Requiring real solutions, and that $W \to 0$ when $x \to \infty$, we find

$$W = A \exp[-K_1(x - L)] + B \exp[-K_2(x - L)] \cos[K_3(x - L)] + C \exp[-K_2(x - L)] \sin[K_3(x - L)]. \tag{50}$$

The real constants K_1, K_2, and K_3 are related to the three admissible roots r_1, r_2, and r_3 through

$$r_1 = -K_1, \ r_2 = -K_2 - iK_3, \ r_3 = -K_2 + iK_3. \tag{51}$$

They are readily determined from (49). The real constants A, B, and C are obtained from requiring continuity of vertical velocity and shear stress at $x = L$, plus the conservation of volume. For the marginally stable vertical symmetric mode, this last condition can be stated as

$$\int_0^L w_1 dx + \int_L^\infty w_2 dx = 0, \ z = 1/2. \tag{52}$$

In Fig. 2, we have depicted the matched solution for the non-dimensional vertical velocity when we have marginal instability in the ascending zone and three different values for the non-dimensional stability in the descending zone.

From Fig. 2, we note that increasing stability makes the descending part of the cell wider, as well as decreasing the numerical value of the negative vertical velocity. From the definition $R = R_\gamma - R_N$, we have that $R_N = R_c$ (dashed line) corresponds to the case when $R_\gamma = 2R_N$ ($\rho_m \gamma$ is twice as large as the numerical value of the environmental density gradient). In fact, when $R_N \to 0$, we note from (49) that the only admissible solution $r = -\pi$ is, in fact, a triple root. This means that the solution (50) in this case must be

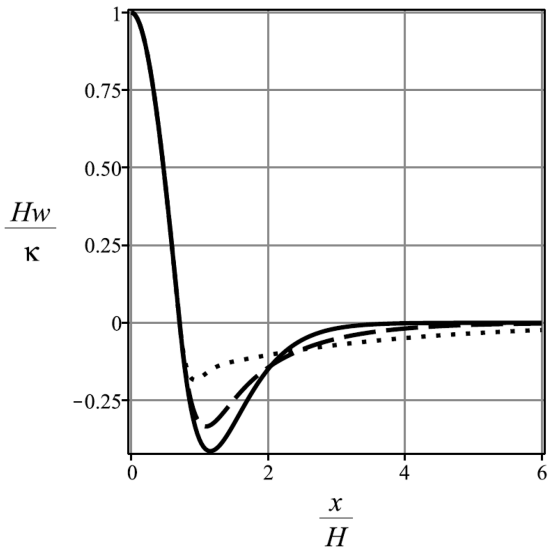

FIG. 2. Non-dimensional vertical velocity distribution near the ice wall ($x \ge 0$, $z = 1/2$), at the onset of convection, i.e., $R = R_c = 27\pi^4/4$ in the unstable region. In the stable region ($w < 0$), the various graphs are for $R_N = 0.01R_c$ (solid line), $R_N = R_c$ (dashed line), and $R_N = 10R_c$ (dotted line).

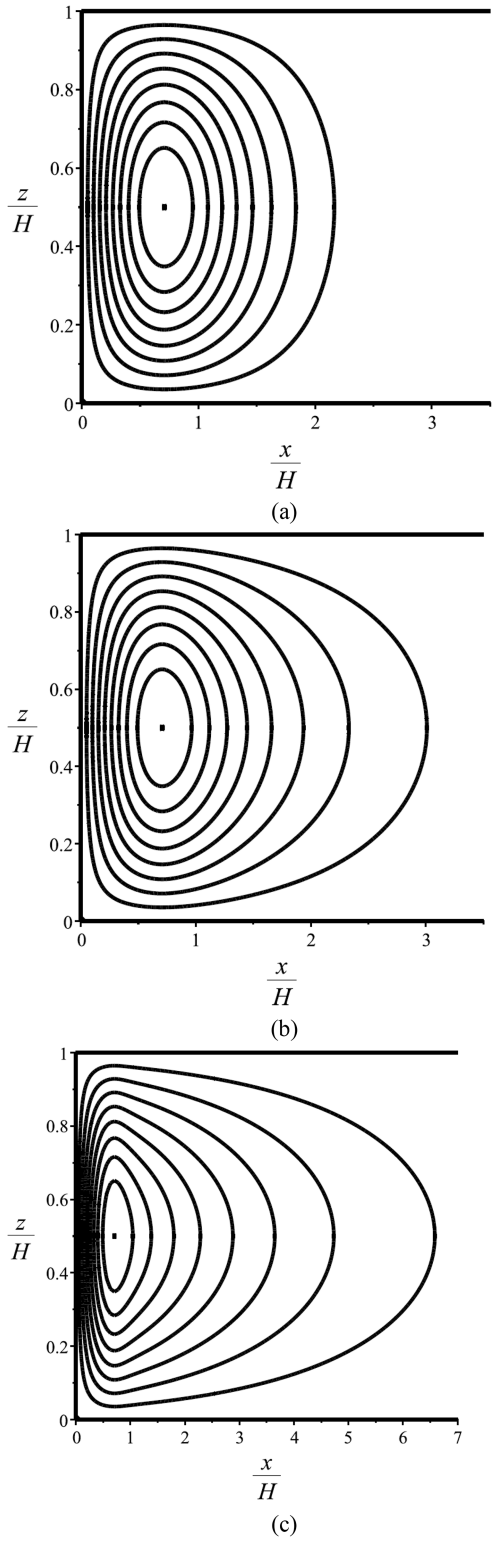

FIG. 3. (a) Stream function for marginal instability when $R_N = 0$. (b) The stream function for marginal instability when $R_N = R_c$. (c) The stream function for marginal instability when $R_N = 10R_c$.

replaced by

$$W = \left[A + B(x-L) + C(x-L)^2\right]\exp[-\pi(x-L)], \qquad (53)$$

where the coefficients are easily obtained from our former matching conditions. It is readily shown that $A = 0, B = -\pi/2^{1/2}$, and $C = -2^{1/2}\pi^2/4$. In this case, when the area of descending motion is neutrally stable, the width of the descending part of the cell is not very much larger than the ascending part.

In Fig. 3, we have plotted the stream function ψ defined by $u = -\partial\psi/\partial z$ and $w = \partial\psi/\partial x$. Figure 3(a) shows a convection cell for $R_N = 0$ (neutral descending area), Fig. 3(b) shows for the case when $R_N = R_c$, and Fig. 3(c) shows for the case when $R_N = 10R_c$ (strongly stable descending area).

From the plots of the stream function in Figs. 3(a)–3(c), we notice the same feature as seen in Fig. 2, i.e., the fluid always rises in a narrow region and sinks in a much broader region. This is similar to the findings for the atmosphere.[3–5] Again, it is demonstrated that the more stable the region is, the wider the descending area will be. Although we have considered a semi-infinite domain $x \in [0, \infty >$, we note that our cell solutions only occupy a limited fraction, typically 4–6 times the fluid depth.

In the study by Jordan *et al.*,[16] the frazil ice formation is modeled mathematically and coupled to the other dependent variables of the problem (velocity, temperature, and salinity). For given background profiles of mean temperature, salinity, and frazil ice concentration, they compute growth rates for unstable perturbations of this basic system. There are several reasons why the instability analysis[16] does not produce steady convection patterns similar to those shown in Fig. 3. First, for the part of the model study that can be compared to ours (with no inflow and outflow in the bottom layer), they consider a box model, which is 400 m deep (the depth of the ice shelf) and only 200 m wide. With this geometry, it is impossible to capture the marginally unstable convection pattern similar to those shown in Fig. 3, where the width of one cell typically occupies 4–6 times the depth. In addition, they initiate their numerical calculations with a thin layer (20 m) of constant frazil ice concentration and relatively warm water (above the freezing point) at the bottom of the box. This constitutes a low-density bottom layer, which very soon becomes convectively unstable. The resulting flow pattern at small times (their Fig. 5) has a lateral dimension of the order of the thickness of the bottom layer. Obviously, this is a different problem from the one studied in our paper.

VII. NONLINEAR MOTION IN A THIN LAYER

In order to investigate the nature of convection arising from conditional instability, we solve the nonlinear governing equations (32)–(34) in a box geometry. For this purpose, we apply the commercial partial differential equation (PDE) solver COMSOL Multiphysics™. The program uses finite elements to solve the PDE system. Here, we use the predefined packages for fluid motion and heat/density transport. In this study, we integrate the model for 5 h, when a near-steady state solution is obtained. In this computation, we can choose R_N and R_γ in (35) and (36) at will as long as $R = R_\gamma - R_N > R_c$. Since the results for moderately supercritical conditions become qualitatively the same, we choose to perform calculations for an adiabatic density lapse rate (22), which is twice as large as the numerical value of the environmental density

gradient (30), i.e., $R_y = 2R_N$. We utilize that

$$U(w) = \frac{1}{2}[1 + \mathrm{sgn}(w)], \tag{54}$$

where the signum function is defined as

$$\mathrm{sgn}(w) = \begin{cases} 1, & w > 0, \\ -1, & w < 0. \end{cases} \tag{55}$$

Then, (34) for the perturbation density can be written for two-dimensional motion as

$$\partial\sigma/\partial t + u\partial\sigma/\partial x + w\partial\sigma/\partial z + R[\mathrm{sgn}(w)]w = \partial^2\sigma/\partial x^2 + \partial^2\sigma/\partial z^2. \tag{56}$$

To simulate convection in a turbulent ocean, we take that $P_r = 1$. The equations for the conservation of momentum and volume now reduce to

$$\partial u/\partial t + u\partial u/\partial x + w\partial u/\partial z = -\partial p/\partial x + \partial^2 u/\partial x^2 + \partial^2 u/\partial z^2, \tag{57}$$

$$\partial w/\partial t + u\partial w/\partial x + w\partial w/\partial z = -\partial p/\partial z - \sigma + \partial^2 w/\partial x^2 + \partial^2 w/\partial z^2, \tag{58}$$

$$\partial u/\partial x + \partial w/\partial z = 0. \tag{59}$$

We perform our calculations in a rectangular box, where the length is much larger than the height. The dimensional length of the model is l, and we have vertical end-walls at $x = 0$ and $x = a$, where $a = l/H \gg 1$ is the aspect ratio. At the horizontal boundaries, we use no-slip and perfectly conducting conditions, that is,

$$u = w = \sigma = 0, \quad z = 0, \quad 1. \tag{60}$$

We take that the end-walls are insulating, so here,

$$u = w = \partial\sigma/\partial x = 0, \quad x = 0, a. \tag{61}$$

In the model, we use water as the working fluid and use temperature instead of density. The model is driven by applying the fixed temperatures $\Delta T/2$ and $-\Delta T/2$ at the lower and upper boundaries, respectively. The relevant Rayleigh number for this problem then becomes $R = g\alpha_m \Delta T H^3/(\kappa\nu)$. Test results obtained for ordinary Rayleigh–Benard convection, i.e., by replacing the signum function in (56) by 1, gave regularly spaced convection cells when $a = 10$, and $R \geq R_c = 1708$, which is the critical Rayleigh number for perfectly conducting, no-slip horizontal boundaries.[25] In Fig. 4, we have depicted this situation for $R = 1400$ ($\Delta T = 0.1$ K) (upper panel, conduction only) and the steady stream lines for slightly supercritical motion $R = 2100$ ($\Delta T = 0.15$ K) (lower panel).

In the case of conditional instability, obtained by retaining the signum function in (56), the spacing between the cells became much larger, as expected. In Fig. 5, we have depicted the steady cell pattern for $R = 7000$ ($\Delta T = 0.5$ K) and $R = 10\,500$($\Delta T = 0.75$ K).

By comparing Figs. 4 and 5, we note the striking difference between the cell patterns in ordinary Rayleigh–Benard convection, and when conditional instability occurs.

The relevance of these nonlinear numerical calculations to our ice shelf problem is that the qualitative picture of narrow ascending regions and much broader sinking regions prevails; see, e.g., Fig. 2. In each of the cells in Fig. 5, the rising motion in the middle can represent the motion near the vertical shelf front. Even if the boundary conditions are different (free-slip vs no-slip), we note by comparing Figs. 2 and 5 that the ratio of the width of the sinking region to the width of the ascending region for each half-cell is of the order 6–8 in both cases.

Even with relatively high values for the turbulent eddy coefficients, the destabilizing Rayleigh number (37) often becomes much larger than the critical value for the onset of convection. This applies

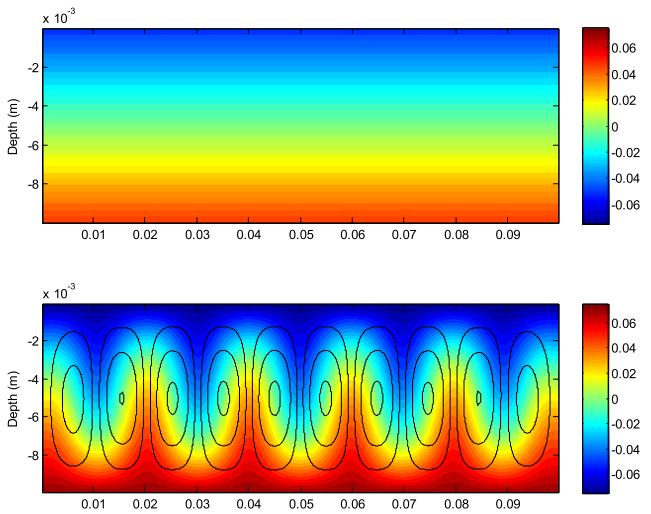

FIG. 4. Temperature and stream function (solid black lines) for the Rayleigh–Benard problem. Upper panel: $R = 1400$ (pure conduction). Lower panel: slightly supercritical convection ($R = 2100$). The color scale on the right-hand side depicts temperature deviations in K. The calculations are made in a box geometry with an aspect ratio $a = 10$.

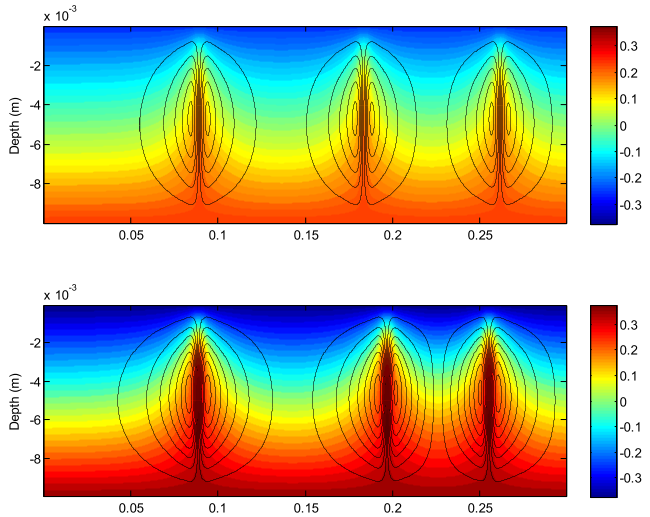

FIG. 5. Temperature and stream function (solid black lines) for nonlinear convection in the case of conditional instability when $R = 7000$ (upper panel) and $R = 10\,500$ (lower panel). The color scale on the right-hand side depicts temperature deviations in K. The calculations are made in a box geometry with an aspect ratio $a = 30$.

to the atmosphere as well as the ocean and means that this problem, in reality, is very nonlinear. Therefore, the present calculations for moderately supercritical Rayleigh numbers can only yield a qualitatively picture of this important convection process.

VIII. DISCUSSION AND CONCLUDING REMARKS

Convective motions in nature (e.g., cloud formation) tend to be three-dimensional. However, the present idealized model of a vertical ice shelf front, with a relatively small region of supercooled water in the seaward direction, favors two-dimensional motion. The cellular convective motion due to conditional instability will increase the mixing in the region close to the ice shelf front, and the vertical transport of nutrient water from deeper layers may enhance the primary biological production in the surface layer.

In moist atmospheric convection, heavy water droplets fall out of the air as precipitation during ascent or at the cloud base. In the ocean, the salinity increase in a rising water parcel due to ice crystal formation will lead to a density increase near the surface when the crystals leave the parcel and form a surface ice cover or adhere to the already present surface ice.[8] This is also shown to happen in the model studied by Jordan *et al.*[16] We realize from our calculations that the primary conditional convection process will induce a horizontal transport of the secondary produced salt underneath the ice over a distance, which is large compared with the depth of the layer. This will lead to a salinity boundary layer beneath the ice, which will grow thicker in time. In turn, haline convection may commence when the Rayleigh number based on the boundary-layer thickness exceeds a critical value, causing small-scale vertical mixing in the upper layer.[26] Finally, this process may transport salt water down to the shelf bottom.[8] However, the convective mixing may in turn disturb the formation of supercooled water and hence the frazil ice production.

Then, the primary process of conditional convection will halt and so will the production of saline surface water. This negative feedback indicates that the shelf-water formation by conditional instability is indeed an intermittent process.

ACKNOWLEDGMENTS

Financial support from the Research Council of Norway under Grant No. 280625 (Dynamics of floating ice) is gratefully acknowledged.

DATA AVAILABILITY

Data sharing is not applicable to this article as no new data were created or analyzed in this study.

REFERENCES

[1]Lord Rayleigh, "On convection in a horizontal layer of fluid when the higher temperature is on the under side," Philos. Mag. **32**, 529–546 (1916).
[2]D. K. Lilly, "On the theory of unstable disturbances in a conditionally unstable atmosphere," Mon. Weather Rev. **88**(1), 1–17 (1960).
[3]H. L. Kuo, "Convection in a conditionally unstable atmosphere," Tellus **13**, 441–459 (1961).
[4]H. L. Kuo, "Further studies of the properties of cellular convection in a conditionally unstable atmosphere," Tellus **17**, 413–433 (1965).
[5]C. S. Bretherton, "A theory for nonprecipitating moist convection between two parallel plates. Part I: Thermodynamics and 'linear' solutions," J. Atmos. Sci. **44**, 1809–1827 (1987).
[6]C. S. Bretherton, "A theory for nonprecipitating moist convection between two parallel plates. Part II: Nonlinear theory and cloud field organization," J. Atmos. Sci. **45**, 2391–2415 (1988).
[7]B. Stevens, "Atmospheric moist convection," Annu. Rev. Earth Planet. Sci. **33**, 605–643 (2005).
[8]A. Foldvik and T. Kvinge, "Conditional instability of sea water at the freezing point," Deep-Sea Res. **21**, 169–174 (1974).
[9]G. Dieckmann, G. Rohardt, H. Hellmer, and J. Kipfstuhl, "The occurrence of ice platelets at 250 m depth near the Filchner ice shelf and its significance for sea ice biology," Deep-Sea Res. **33**, 141–148 (1986).
[10]P. A. Hunkeler, M. Hoppmann, S. Hendricks, T. Kalscheuer, and R. Gerdes, "A glimpse beneath Antarctic sea ice: Platelet layer volume from multifrequency electromagnetic induction sounding," Geophys. Res. Lett. **43**, 222–231, https://doi.org/10.1002/2015gl065074 (2016).
[11]L. H. Smedsrud and A. Jenkins, "Frazil ice formation in an ice shelf water plume," J. Geophys. Res.: Oceans **109**, C03025, https://doi.org/10.1029/2003jc001851 (2004).
[12]D. W. Rees Jones and A. J. Wells, "Frazil-ice growth rate and dynamics in mixed layers and sub-ice-shelf plumes," Cryosphere **12**, 25–38 (2018).
[13]E. G. Morozov, A. V. Marchenko, and Y. V. Fomin, "Supercooled water near the glacier front in Spitsbergen," Izv., Atmos. Oceanic Phys. **51**, 203–207 (2015).
[14]A. V. Marchenko, E. G. Morozov, and N. A. Marchenko, "Supercooling of seawater near the glacier front in a Fjord," Earth Sci. Res. **6**, 97–108 (2017).
[15]R. Skogseth, F. Nilsen, and L. H. Smedsrud, "Supercooled water in an Arctic polynya: Observations and modeling," J. Glaciol. **55**, 43–52 (2009).
[16]J. R. Jordan, S. Kimura, P. R. Holland, A. Jenkins, and M. D. Piggott, "On the conditional frazil ice instability in seawater," J. Phys. Oceanogr. **45**, 1121–1138 (2015).
[17]H. N. Shirer and J. A. Dutton, "The branching hierarchy of multiple solutions in a model of moist convection," J. Amos. Sci. **36**, 1705–1721 (1979).
[18]G. J. Haltiner and R. T. Williams, *Numerical Prediction and Dynamic Meteorology*, 2nd ed. (John Wiley & Sons, New York, 1980), p. 477.
[19]X.-Y. Huang and E. Källén, "A low-order model for moist convection," Tellus **38A**, 381–396 (1986).
[20]E. A. Spiegel and G. Veronis, "On the Boussinesq approximation for a compressible fluid," Astrophys. J. **131**, 442–447 (1960).
[21]A. Jenkins and A. Bombosch, "Modeling the effect of frazil ice crystals on the dynamics of ice shelf water plumes," J. Geophys. Res. **100**, 6967–6981, https://doi.org/10.1029/94jc03227 (1995).
[22]T. B. Løyning and J. E. Weber, "Thermobaric effect on buoyancy-driven convection in cold seawater," J. Geophys. Res. **102**, 27875–27885, https://doi.org/10.1029/97jc02549 (1997).
[23]A. E. Gill, *Atmosphere-Ocean Dynamics* (Academic Press, 1982).
[24]E. Palm, "Nonlinear thermal convection," Annu. Rev. Fluid Mech. **7**, 39–61 (1975).
[25]S. Chandrasekhar, *Hydrodynamic and Hydromagnetic Stability* (Oxford University Press, 1961).
[26]T. D. Foster, "Haline convection in polynyas and leads," J. Phys. Oceanogr. **2**, 462–469 (1972).